inorganics

MDPI

Article

Scalable High-Yield Exfoliation of Hydrophilic h-BN Nanosheets via Gallium Intercalation

Sungsan Kang [1], Dahun Kim [1], Seonyou Park [1], Sung-Tae Lee [1], John Hong [2], Sanghyo Lee [3,*] and Sangyeon Pak [1,*]

[1] School of Electronic and Electrical Engineering, Hongik University, Seoul 04066, Republic of Korea; b615003@g.hongik.ac.kr (S.K.); rlaekgns0221@mail.hongik.ac.kr (D.K.); ssunyu51@g.hongik.ac.kr (S.P.); lst777@hongik.ac.kr (S.-T.L.)
[2] School of Materials Science and Engineering, Kookmin University, Seoul 02707, Republic of Korea; johnhong@kookmin.ac.kr
[3] School of Materials Science and Engineering, Kumoh National Institute of Technology, Gumi 39177, Republic of Korea
* Correspondence: sanghyo.lee@kumoh.ac.kr (S.L.); spak@hongik.ac.kr (S.P.)

Abstract

Hexagonal boron nitride (h-BN) possesses a unique combination of a wide bandgap, high thermal conductivity, and chemical inertness, making it a key insulating and thermal management material for advanced electronics and nanocomposites. However, its intrinsic hydrophobicity and strong interlayer van der Waals forces severely limit exfoliation efficiency and dispersion stability, particularly in scalable liquid-phase processes. Here, we report a synergistic exfoliation strategy that integrates acid-induced hydroxylation with gallium (Ga) intercalation to achieve high-yield (>80%) production of ultrathin (<4 nm) hydrophilic h-BN nanosheets. Hydroxylation introduces abundant -OH groups, expanding interlayer spacing and significantly increasing surface polarity, while Ga intercalation leverages its native Ga_2O_3 shell to form strong interfacial interactions with hydroxylated basal planes. This oxide-mediated adhesion facilitates efficient layer separation under mild sonication, yielding nanosheets with well-preserved lateral dimensions and exceptional dispersion stability in polar solvents. Comprehensive characterization confirms the sequential chemical and structural modifications, revealing the crucial roles of hydroxylation-induced activation and Ga_2O_3 assisted wettability enhancement. This combined chemical activation–soft metallic intercalation approach provides a scalable, solution-processable route to high-quality h-BN nanosheets, opening new opportunities for their integration into dielectric, thermal interface, and multifunctional composite systems.

Keywords: boron nitride; h-BN; hydrophilic; liquid exfoliation; gallium intercalation

check for updates

Academic Editors: Martina Vrankić and Melita Menelaou

Received: 27 August 2025
Revised: 11 September 2025
Accepted: 23 September 2025
Published: 25 September 2025

Citation: Kang, S.; Kim, D.; Park, S.; Lee, S.-T.; Hong, J.; Lee, S.; Pak, S. Scalable High-Yield Exfoliation of Hydrophilic h-BN Nanosheets via Gallium Intercalation. *Inorganics* **2025**, *13*, 314. https://doi.org/10.3390/inorganics13100314

Copyright: © 2025 by the authors. Licensee MDPI, Basel, Switzerland. This article is an open access article distributed under the terms and conditions of the Creative Commons Attribution (CC BY) license (https://creativecommons.org/licenses/by/4.0/).

1. Introduction

Two-dimensional (2D) materials have emerged as pivotal factors in advanced technologies owing to their exceptional electrical, thermal, and mechanical properties [1–5]. Among them, hexagonal boron nitride (h-BN) is particularly notable for its wide bandgap (~6 eV) [6], high in-plane thermal conductivity [7], outstanding chemical and thermal stability [8], and electrical insulation [9]. Its unique combination of properties makes h-BN an ideal candidate for use as a dielectric layer, thermal interface material [10,11], protective coating [12–14], and electrically insulating filler in polymer composites [15]. Furthermore, its atomically smooth surface and compatibility with other 2D materials have positioned it

as a critical component in van der Waals heterostructures for next-generation electronic and photonic devices [16,17].

However, despite extensive efforts to develop reliable exfoliation strategies for hexagonal boron nitride, achieving high yield and precise control over nanosheet morphology at scale remains a significant challenge [18,19]. A variety of approaches, including mechanical shearing, ball milling [18], chemical oxidation [20–23], ion intercalation [24], and sonication-assisted liquid-phase exfoliation [25], have been explored to delaminate bulk crystals into nanosheets. While these methods have provided valuable insights, they are frequently hindered by limited exfoliation efficiency typically below 10–20% and often produce broad thickness distributions or reduced lateral sizes due to structural degradation during processing. Moreover, the inherently hydrophobic nature of pristine h-BN severely restricts its dispersion stability in polar solvents [26–29], thereby impeding both the delamination process and subsequent solution-based processing. This limitation highlights the importance of strategies that not only weaken interlayer interactions but also introduce surface functionalities to render h-BN hydrophilic, enabling more stable dispersions and higher exfoliation yields in liquid-phase processes [30].

Recent studies have shown that strategies such as defect induction, heteroatom incorporation, and oxide-mediated interactions can effectively regulate interlayer spacing in layered materials, thereby enhancing exfoliation efficiency and stability. Building on these insights, pre-functionalization via hydroxylation has emerged as a promising strategy for h-BN to weaken interlayer van der Waals forces, enhance hydrophilicity, and improve compatibility with subsequent exfoliation media [31–34].While effective in principle, such chemical activation approaches often suffer from slow reaction kinetics, limited hydroxylation selectivity, and scalability challenges. In parallel, liquid metal-based intercalation particularly using gallium or Galinstan has gained attention for 2D material processing due to its self-limiting oxide shell and high interfacial reactivity, which can facilitate the formation of adhesive networks that penetrate and delaminate layered structures [35,36]. However, despite its potential, the integration of liquid metal intercalation with chemically pre-activated h-BN remains underexplored, particularly in the context of achieving high exfoliation yield under scalable and mild processing conditions.

Here, we report a synergistic exfoliation strategy that integrates acid-induced hydroxylation with gallium-mediated intercalation to enable liquid-phase exfoliation of hexagonal boron nitride with both exceptional hydrophilicity and high yield. Hydroxylation introduces abundant surface -OH groups, markedly enhancing surface polarity and wettability, thereby facilitating stable dispersion in polar solvents. The subsequent infiltration of gallium, a low-melting-point liquid metal, leverages its oxide-mediated adhesion to promote clean and efficient layer separation under mild conditions. This combined approach not only produces nanosheets with significantly improved hydrophilicity, reduced thickness, and well-preserved lateral dimensions but also achieves a remarkable exfoliation yield exceeding 80%, consistently yielding h-BN powders thinner than 4 nm. Such performance represents a substantial advancement over conventional exfoliation techniques, as further detailed in Table S1. Our findings establish a new paradigm for scalable 2D material production by uniting chemical activation with soft metallic intercalation, offering a broadly applicable route for the mass production of hydrophilic h-BN nanosheets for use in thermal management, dielectric insulation, and nanocomposite engineering.

2. Results and Discussion

To enable efficient and scalable exfoliation of h-BN, we adopted a sequential strategy of acid-induced hydroxylation followed by gallium (Ga) intercalation (Figure 1a). The rationale behind this approach is twofold: hydroxylation introduces polar -OH groups

that expand the interlayer spacing and increase surface polarity, thereby enhancing compatibility with liquid metal; subsequently, Ga intercalation exploits the strong adhesion of its native oxide layer to these polar sites, enabling gentle yet effective layer separation under mild processing conditions. This combination is designed to overcome the limitations of conventional exfoliation techniques, which often suffer from low yield, incomplete delamination, and poor control over nanosheet morphology.

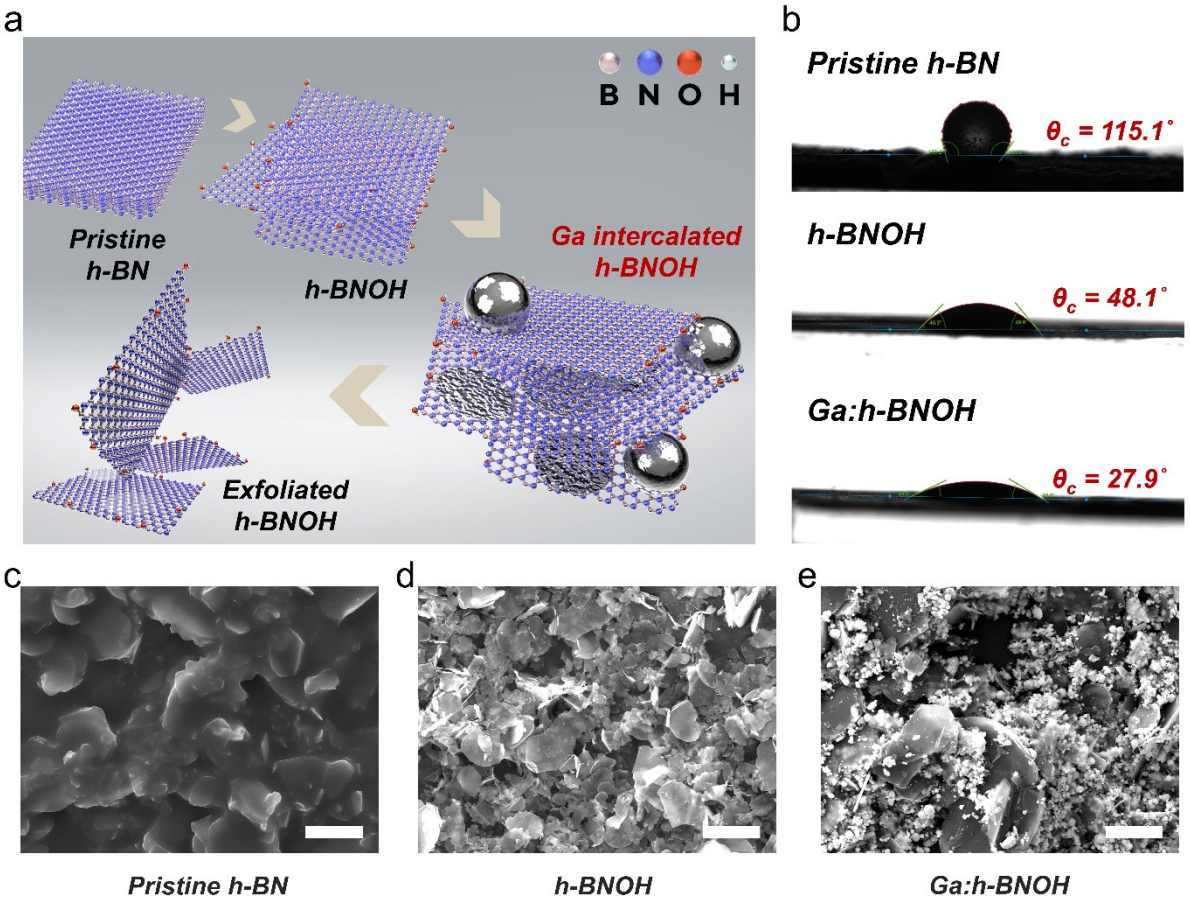


Figure 1. (**a**) Schematic illustration of the sequential hydroxylation and gallium intercalation-assisted liquid-phase exfoliation process for h-BN nanosheets. (**b**) Water contact angle measurements showing the progressive enhancement in surface hydrophilicity. FE-SEM images of (**c**) pristine h-BN, (**d**) h-BNOH, and (**e**) Ga-intercalated h-BNOH (Scale bar = 10 μm).

Surface wettability measurements clearly demonstrate the progressive chemical modification achieved through the sequential hydroxylation and Ga intercalation steps (Figure 1b). Contact angle analysis revealed that pristine h-BN exhibits a high contact angle of 115.1°, characteristic of its intrinsically hydrophobic basal planes and low surface polarity [26]. Following hydroxylation, Hydroxylated h-BN (h-BNOH) exhibited a sharp decrease in contact angle to 48.1°, indicating the successful incorporation of hydrophilic -OH functional groups, which increase surface polarity and improve interaction with polar solvents [37,38]. Subsequent Ga intercalation produced Ga intercalated and Exfoliated h-BNOH (Ga:h-BNOH), which further reduced the contact angle to 27.9°, representing a level of hydrophilicity that suggests strong affinity for aqueous environments and the potential for stable dispersion in polar media [27]. This stepwise reduction in contact angle directly correlates with the targeted chemical modifications, confirming that each stage in the process contributes to enhancing the surface chemistry in a manner conducive to efficient exfoliation.

Complementary morphological characterization using field-emission scanning electron microscopy (FE-SEM) further corroborates the structural transformation induced by the hydroxylation-Ga intercalation sequence (Figure 1c). Pristine h-BN powders present as densely packed, smooth-surfaced platelets with minimal evidence of delamination. After hydroxylation, the particles exhibit a more fragmented appearance, with smaller, irregularly shaped flakes and roughened surfaces, consistent with partial interlayer disruption and the introduction of defect sites. Ga intercalation produces a markedly different morphology, characterized by a porous, loosely stacked architecture and clearly separated thin flakes, indicative of extensive layer exfoliation. The combination of enhanced surface polarity and mechanical delamination facilitated by Ga infiltration enables the production of nanosheets with an average thickness of around 4 nm and yields exceeding 80%, offering material characteristics ideally suited for scalable solution processing and integration into advanced composite and coating systems.

The evolution of chemical bonding during the sequential hydroxylation and gallium intercalation process was first examined by Fourier-transform infrared (FTIR) spectroscopy (Figure 2a,b). In the full spectra, pristine hexagonal boron nitride exhibits the characteristic B-N stretching (~1365 cm^{-1}) and B-N-B bending (~812 cm^{-1}) modes, consistent with its layered crystalline structure. Upon hydroxylation, an additional broad absorption band appears in the range of 3200–3500 cm^{-1}, which can be attributed to the stretching vibrations of surface -OH groups introduced at defect and edge sites [39,40]. This modification further induces subtle intensity changes in the B-N-B bending mode, suggesting partial distortion of the in-plane lattice. Subsequent Ga-assisted exfoliation gives rise to new absorption features in the low-wavenumber region, including bands assignable to Ga-O-H and Ga-O-Ga vibrations, indicative of both oxide-bound gallium species and intercalated metallic Ga domains [41]. The presence of Ga-O-Ga vibrations in particular evidences the formation of Ga_2O_3, whose polar nature further enhances the hydrophilicity of exfoliated h-BNOH by increasing surface energy and affinity toward polar solvents [42]. The zoomed-in spectra clearly resolve these emerging peaks, confirming the successful incorporation of gallium-derived oxides that collectively contribute to interlayer expansion, improved wettability, and efficient exfoliation.

To investigate the elemental composition and validate the incorporation of oxygen functionalities and gallium species during the sequential modification, X-ray photoelectron spectroscopy (XPS) survey spectra were collected (Figure 2c). Pristine h-BN exhibits only the characteristic B 1s and N 1s signals, consistent with its stoichiometric composition and chemical inertness. After hydroxylation, the O 1s peak intensity markedly increases [21], accompanied by a minor C 1s contribution, confirming the introduction of oxygen-containing groups such as -OH and B-O bonds at defect and edge sites. In the Ga:h-BNOH sample, in addition to strong B 1s, N 1s, and O 1s peaks, distinct Ga-related features (Ga 2p, Ga 3p, and Ga 3d) emerge, which are completely absent in pristine and hydroxylated h-BN. The presence of these gallium signals provides direct evidence that liquid Ga has successfully penetrated and intercalated into the hydroxylated structure, while its native oxide shell (Ga_2O_3) further contributes to the overall oxygen content. In particular, the deconvoluted Ga 3d and O 1s spectra of Ga:h-BNOH (Figure S1) clearly resolved distinct Ga-O bonding states, thereby confirming the presence of the Ga_2O_3 layer within the intercalated structure. This analysis was performed to unambiguously distinguish Ga-O contributions from overlapping signals and thus verify the oxide's incorporation. Previous studies have quantitatively demonstrated that the adhesion energy between h-BN and Ga_2O_3 (≈0.275 J m^{-2}) exceeds that of intrinsic h-BN bilayers (≈0.231 J m^{-2}), indicating that the Ga_2O_3 skin substantially enhances interfacial adhesion beyond the native interlayer forces of h-BN [35]. This evolution of spectral features confirms that hydroxylation not only enhances surface

polarity but also creates chemically active interfaces that are compatible with gallium infiltration, thereby enabling efficient interlayer expansion and high-yield exfoliation.

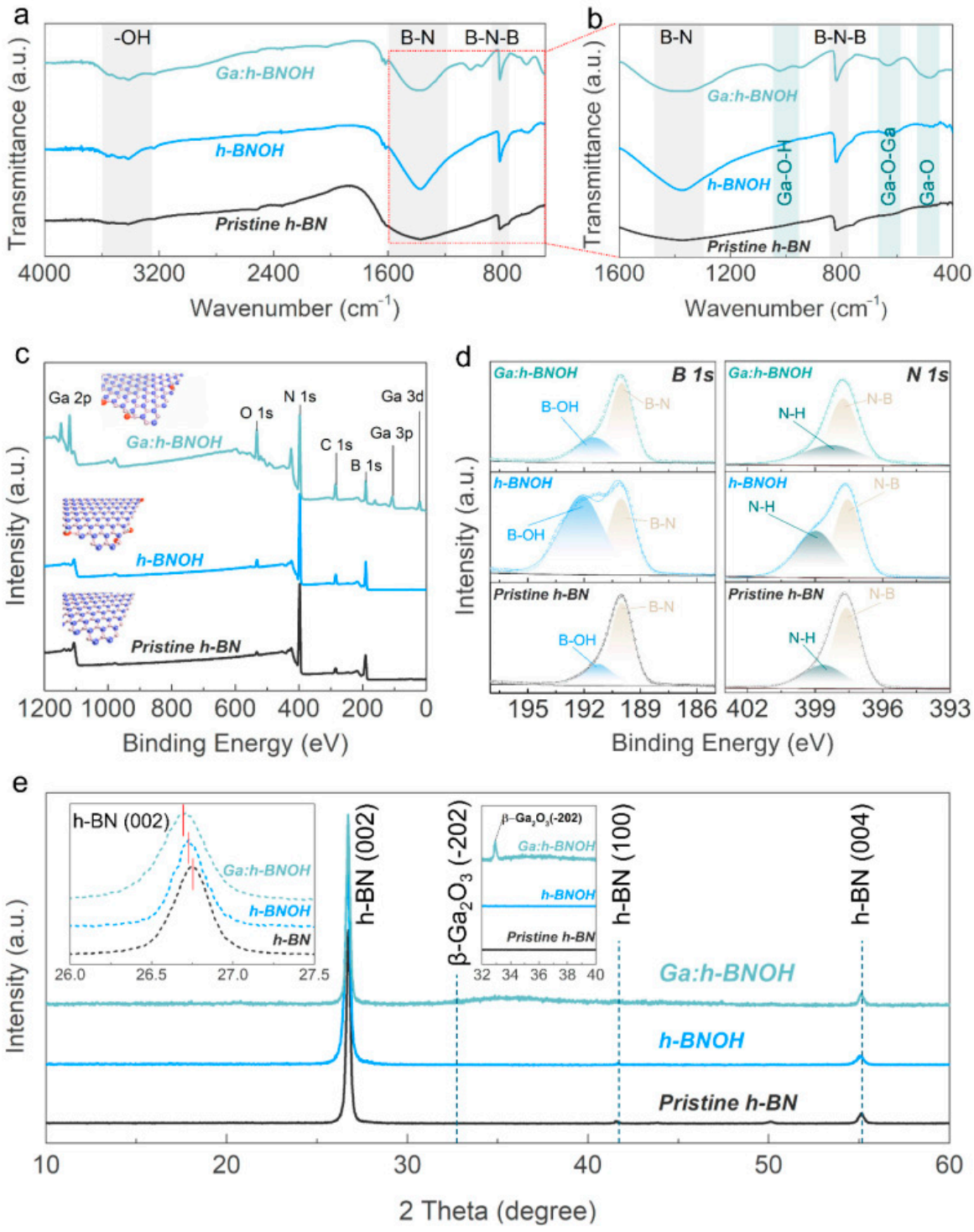


Figure 2. (**a**) FTIR spectra of pristine h-BN, h-BNOH, and Ga:h-BNOH. (**b**) Zoomed FTIR region. (**c**) XPS survey spectra and (**d**) High-resolution B 1s, N 1s revealing B-OH bond formation in h-BNOH and Ga:h-BNOH. (**e**) XRD patterns showing the (002) peak shift to lower 2θ after hydroxylation, retention of expanded interlayer spacing after gallium intercalation, and the appearance of the Ga_2O_3 (402) reflection.

To gain deeper insights into the bonding configurations of boron and nitrogen high-resolution XPS measurements were carried out (Figure 2d). In the B 1s spectra, pristine

h-BN shows a dominant B-N peak at ~190 eV, consistent with its crystalline lattice. Upon hydroxylation, additional oxygen-related components emerge, including a B-OH contribution at 191~192 eV and a weaker feature that can be assigned to B-O bond states [43]. These results confirm that hydroxylation activates boron sites toward both hydroxyl and oxo terminations, in line with the substantial increase in hydrophilicity observed in contact angle measurements (from 115.1° for pristine h-BN to 48.1° for h-BNOH). In Ga:h-BNOH, the B 1s spectra does not simply show a monotonic increase in the B-O signal; instead, oxygen is rebalanced between B-O(H) and Ga-O environments. This redistribution leads to a relatively lower B-O peak intensity compared to h-BNOH, while the overall B 1s envelope becomes broadened due to the coexistence of multiple oxygenated states. The presence of Ga_2O_3 is particularly significant (Figure 2c), as its polar nature enhances surface wettability, consistent with the further reduction in the contact angle to 27.9°. Taken together, these observations suggest that hydroxylation-induced B-OH/B-O formation, coupled with gallium oxide-mediated polarity enhancement, synergistically drives interfacial adhesion and efficient layer delamination during exfoliation.

To investigate the crystallographic evolution and variation in interlayer spacing induced by sequential hydroxylation and gallium intercalation, X-ray diffraction (XRD) measurements were performed (Figure 2e). The pristine hexagonal boron nitride displays a sharp and intense (002) diffraction at ~26.8°, characteristic of its highly ordered layered stacking. Following hydroxylation, the (002) reflection undergoes a discernible shift toward lower 2θ (~26.6°) accompanied by peak broadening, indicative of an expanded d-spacing arising from the incorporation of hydroxyl functionalities at basal edges and defect sites [44–46]. Such lattice expansion is in good agreement with the FTIR signatures of-OH stretching vibrations and the XPS-derived evidence of B-O bonding, collectively confirming successful surface functionalization. Upon subsequent gallium intercalation, the (002) peak position remains at the expanded angle, signifying the preservation of the increased interlayer distance, while an additional reflection assignable to the (-202) plane of gallium oxide (Ga_2O_3) becomes evident [35,47]. The appearance of this oxide phase is consistent with the Ga 3d XPS spectra and supports the proposed mechanism in which the native oxide layer of gallium forms strong interfacial interactions via hydrogen bonding or coordination with the hydroxyl groups on h-BNOH surfaces. These enhanced adhesion forces promote deeper penetration of gallium into the interlayers and facilitate more effective mechanical separation during agitation, thereby improving the overall exfoliation efficiency. Taken together, the XRD, FTIR, and XPS analyses provide converging evidence for the formation of chemically expanded and gallium-intercalated h-BN structures, structurally and chemically optimized for high-yield liquid-phase exfoliation.

To optimize the gallium intercalation process, we systematically varied the mixing ratio between hydroxylated h-BN (h-BNOH) and liquid Ga, as shown in Figure 3a–c. The objective was to identify the ratio at which intercalation proceeds most efficiently while minimizing residual metallic Ga. A time-lapse image showing morphological evolution (Figure 3d) revealed that Ga gradually penetrates into the h-BNOH matrix within 24 h, forming increasingly dark dispersions. After centrifugation (Figure 3e), excess Ga could be removed, leaving behind stable dispersions of Ga:h-BNOH [35]. Notably, as the Ga content increased, a saturation trend was observed: the 1:1 ratio already provided sufficient Ga for effective intercalation, while the 1:2 ratio resulted in visible amounts of unreacted Ga metal that could not be incorporated into the layered galleries. This indicates that beyond a certain threshold, additional Ga does not enhance intercalation but rather accumulates as excess bulk metal. Collectively, these observations confirm that a stoichiometric balance between Ga and h-BNOH is crucial, with the 1:1 ratio representing the optimal condition for achieving efficient and uniform intercalation.

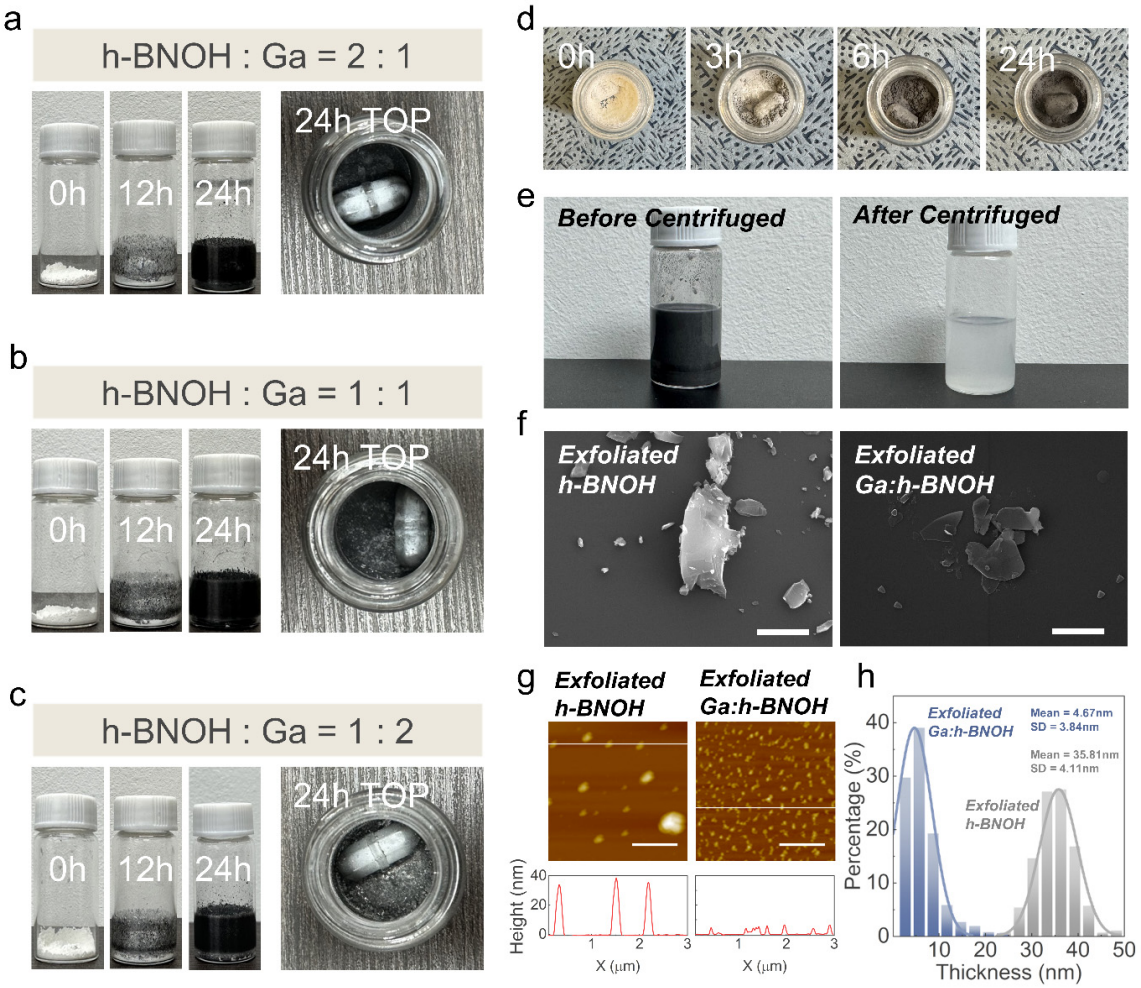


Figure 3. Optimization of Gallium assisted exfoliation process. (**a**–**c**) Photographs of h-BNOH mixed with Ga at different mass ratios (h-BNOH:Ga = 2:1, 1:1, and 1:2) (**d**) Time-dependent photographs (0–24 h) during Ga intercalation. (**e**) Dispersions before and after centrifugation. (**f**) FE-SEM images of exfoliated h-BNOH and Ga:h-BNOH (scale bar = 2 μm). (**g**) AFM images and corresponding height profiles of exfoliated h-BNOH and Ga:h-BNOH nanosheets, confirming substantial thickness reduction upon Ga-assisted exfoliation (scale bar = 1 μm). (**h**) Thickness distribution histograms, showing a decrease in mean thickness from ~35.8 nm (h-BNOH) to ~4.7 nm (Ga:h-BNOH).

To evaluate the effect of gallium intercalation on exfoliation efficiency, we compared the morphology and thickness distribution of nanosheets obtained from h-BNOH and Ga:h-BNOH. SEM imaging revealed that exfoliated h-BNOH retained relatively thick and irregular platelet-like structures, whereas Ga:h-BNOH exhibited thinner, more uniform nanosheets with extensive delamination (Figure 3f). AFM characterization further highlighted this contrast: h-BNOH nanosheets displayed broad thickness variations ranging from 20 to 40 nm, while Ga-assisted exfoliation produced nanosheets predominantly within the 3–5 nm range (Figure 3g). This distinction was quantitatively confirmed by statistical thickness histograms, where the average thickness decreased dramatically from ~35.8 nm for h-BNOH to ~4.7 nm for Ga:h-BNOH (Figure 3h). The sharp narrowing of the thickness distribution in the Ga-intercalated samples underscores the enhanced uniformity and efficiency of exfoliation. Taken together, these results demonstrate that Ga intercalation not only facilitates cleaner layer separation but also yields ultrathin nanosheets with superior homogeneity, highlighting its pivotal role in achieving high-yield exfoliation of h-BN.

Also, to evaluate the impact of hydroxylation and gallium intercalation on the wettability and dispersion stability of h-BN, we systematically compared pristine h-BN, h-BNOH,

and Ga:h-BNOH dispersions (Figure 4a–d). As shown in Figure 4a, hydroxylation expands the interlayer spacing, leading to visible volume swelling compared to pristine h-BN, while subsequent Ga intercalation produces a distinct dark-colored dispersion, indicative of gallium incorporation between layers. UV-vis absorption spectra (Figure 4b) further confirm this trend: pristine h-BN shows negligible absorbance due to poor dispersibility, whereas h-BNOH exhibits moderately enhanced absorbance from improved hydrophilicity [21]. In contrast, Ga:h-BNOH displays the highest optical density across the measured wavelength range, reflecting its superior wettability and stable colloidal dispersion. The stability of these dispersions was further evaluated in isopropyl alcohol (IPA). Immediately after dispersion (Figure 4c), all three samples appear suspended, but after one week (Figure 4d), pristine h-BN and h-BNOH show significant sedimentation, while Ga:h-BNOH remains homogeneously dispersed. This long-term stability is attributed to Ga_2O_3 domains deposited along the basal planes, which increase surface energy and introduce polar interaction sites. Collectively, these results confirm that gallium intercalation synergistically enhances the wettability of hydroxylated h-BN, enabling stable and uniform dispersions that are critical for scalable liquid-phase processing.

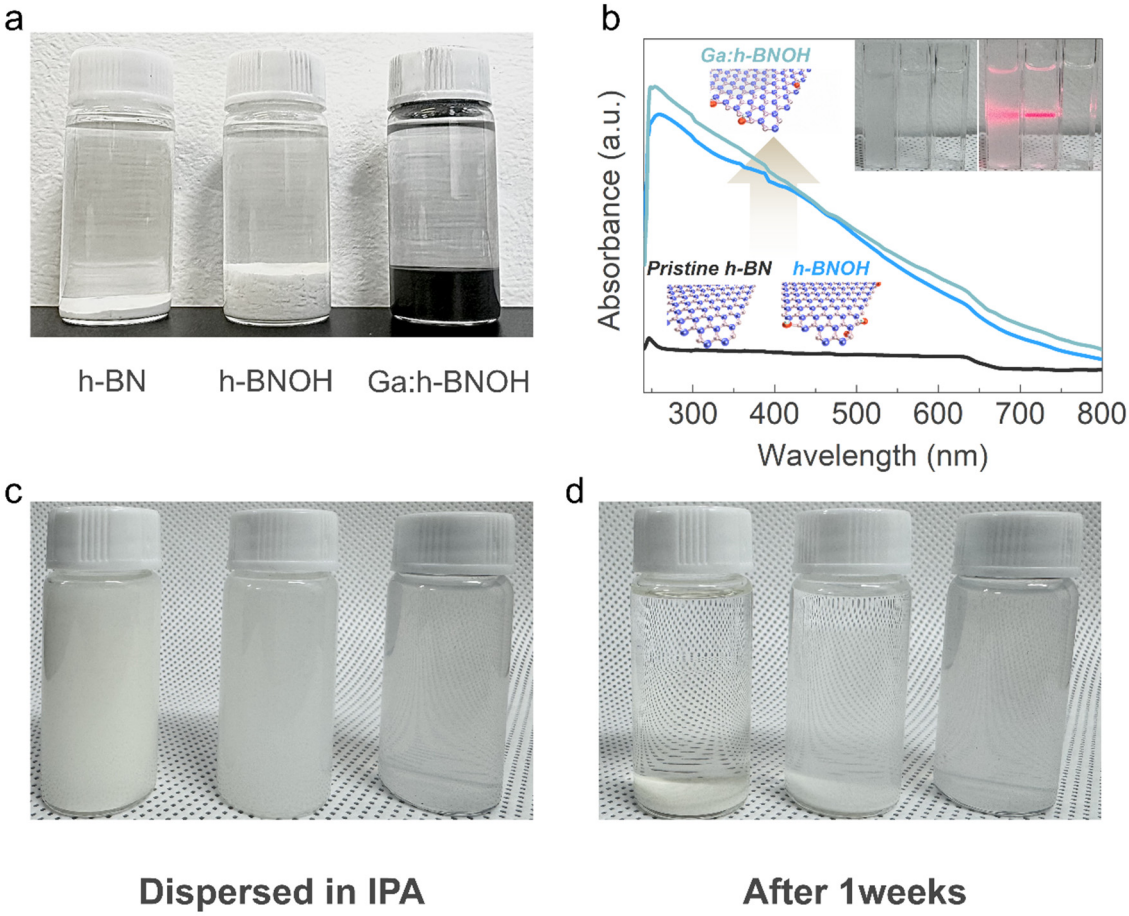


Figure 4. Dispersion behavior and optical properties of h-BN, h-BNOH, and Ga:h-BNOH. (**a**) Photographs of pristine h-BN, h-BNOH, and Ga:h-BNOH powders prior to exfoliation, showing a clear increase in apparent volume after hydroxylation and Ga intercalation due to expanded interlayer spacing. (**b**) UV-vis absorption spectra of dispersions in IPA, revealing significantly enhanced absorbance for h-BNOH and Ga:h-BNOH compared to pristine h-BN. Inset: photographs of dispersions under visible light and a red laser beam. (**c**,**d**) Photographs of the corresponding dispersions in IPA immediately after sonication (**c**) and after one week of storage (**d**), demonstrating that Ga:h-BNOH maintains superior colloidal stability relative to h-BN and h-BNOH.

Finally, to demonstrate the scalability and quantitative efficiency of our exfoliation strategy, we evaluated the volume change, structural evolution, and exfoliation yield of h-BNOH before and after gallium-assisted processing. Hydroxylation alone induced interlayer expansion, consistent with the (002) XRD peak shift (Figure 2e), which resulted in an apparent swelling of powder volume for the same mass. This pre-expanded structure provided a favorable platform for subsequent Ga intercalation, where the oxide-coated liquid metal infiltrated the widened interlayers and promoted efficient layer separation. AFM thickness analysis revealed a clear transition: while h-BNOH nanosheets were predominantly 20–40 nm thick, Ga-assisted exfoliation produced ultrathin nanosheets in the 3–5 nm range. Importantly, the exfoliation yield, calculated by comparing the mass of collected nanosheets after centrifugation with the initial mass of h-BN, consistently exceeded 80%, in line with or surpassing yields reported for other liquid-phase exfoliation methods [18,48,49]. These findings confirm that the integration of hydroxylation and gallium intercalation provides not only superior nanosheet quality but also a scalable and high-yield route for the production of solution-processable, ultrathin h-BN, paving the way for their deployment in thermal management, dielectric insulation, and nanocomposite applications.

3. Materials and Methods

3.1. Materials

Pristine hexagonal boron nitride (h-BN) powders were used as the starting material. Sulfuric acid (H_2SO_4, 98%, GR grade) was purchased from Daejung Chemicals & Metals Co., Ltd. (Siheung-si, South Korea) Gallium metal shots (3 mm, 5N purity) were obtained from ITASCO Inc. via Taewon Scientific Co., Ltd. (Seoul, South Korea) All chemicals were used without further purification. Deionized (DI) water and isopropyl alcohol (IPA, $\geq$99.5%, Daejung Chemicals, Siheung-si, South Korea) were used as solvents for dispersion and washing.

3.2. Hydroxylation of h-BN

Hydroxylated h-BN (h-BNOH) was synthesized via acid-assisted functionalization. In a typical procedure, pristine h-BN powder was dispersed in concentrated sulfuric acid (H_2SO_4, 98%) at a ratio of 10 mg h-BN per mL of acid, and the suspension was magnetically stirred at 80 °C for 12 h to promote surface activation. The selected acid concentration, temperature, and reaction time were optimized to balance effective hydroxyl group introduction with preservation of the h-BN framework, thereby ensuring reproducibility and scalability of the process. The treatment introduces hydroxyl (-OH) groups at defect and edge sites, weakening interlayer van der Waals forces and increasing surface polarity. After reaction completion, the mixture was thoroughly washed with DI water until the pH reached neutral, followed by vacuum drying at 60 °C overnight.

3.3. Gallium Intercalation and Liquid-Phase Exfoliation

The hydroxylated h-BNOH powder was subjected to gallium-assisted intercalation to further expand interlayer spacing and facilitate exfoliation. Liquid gallium (5N, 3 mm shot) was preheated slightly above its melting point (29.8 °C) to ensure complete liquefaction. h-BNOH powder was mixed with the molten gallium in an inert environment and subjected to the mechanical process shown in Figure 3, enabling gallium penetration into the expanded galleries via adhesion of its native oxide layer to polar -OH sites. The gallium h-BNOH mixture was then dispersed in isopropyl alcohol and exfoliated via probe-type ultrasonication (>5 h, 20% amplitude) to delaminate bulk structures into nanosheets.

3.4. Post-Treatment and Product Collection

Following ultrasonication, the dispersion was centrifuged at 3000 rpm for 10 min to remove unexfoliated aggregates. The supernatant, containing well-dispersed gallium-intercalated h-BNOH nanosheets, was collected for further analysis or casting into films. The remaining precipitate was redispersed by ultrasonication and subjected to the same centrifugation procedure, and this cycle was repeated until the sediment became nearly white, ensuring that exfoliated nanosheets were efficiently recovered. This sequential hydroxylation-gallium intercalation-ultrasonication process consistently yielded ultrathin (<4 nm) h-BN nanosheets with an exfoliation yield exceeding 80%.

3.5. Characterization

The morphological characteristics of the samples were analyzed using field-emission scanning electron microscopy (FE-SEM, JEOL JSM-IT710HR, Tokyo, Japan), while atomic force microscopy (AFM, Park Systems XE-100, Suwon, South Korea, tapping mode) was employed to determine nanosheet thickness and surface roughness. Crystallographic structures were examined by X-ray diffraction (XRD, Rigaku Miniflex 600, Tokyo, Japan, Cu Kα radiation, λ = 1.5406 Å). Fourier-transform infrared (FTIR) spectra were obtained using a Thermo Scientific Nicolet iS50 spectrometer (Waltham, MA, USA) in the range of 400–4000 cm^{-1} to identify functional groups. For FTIR measurements, samples were prepared as KBr pellets (KBr:h-BN = 100:1 by weight). X-ray photoelectron spectroscopy (XPS) was performed on a Thermo Scientific ESCALAB 250 system (Waltham, MA, USA) with a monochromatic Al Kα anode (1486.6 eV); binding energies were calibrated to the C 1s peak at 284.8 eV. UV-vis absorption spectra were recorded using a PerkinElmer LAMBDA 365 spectrophotometer (Waltham, MA, USA) with quartz cuvettes, where the dispersions were prepared by suspending h-BN powders in isopropyl alcohol (IPA). Contact angle measurements were performed using a SmartDrop Standard goniometer (FEMTOBIOMED, Seoul, South Korea) to evaluate surface wettability.

4. Conclusions

In this work, we demonstrated a high-yield (>80%) and scalable liquid-phase exfoliation strategy for producing ultrathin (<4 nm) hydrophilic h-BN nanosheets by integrating acid-induced hydroxylation with gallium-assisted intercalation. Hydroxylation effectively expanded the interlayer spacing and introduced abundant -OH groups, markedly enhancing surface polarity, while the subsequent deposition of Ga_2O_3 on the basal planes further increased surface energy and wettability, enabling long-term dispersion stability in polar solvents. Structural and spectroscopic analyses (FTIR, XPS, XRD) confirmed the sequential chemical modifications, and morphological characterization (FE-SEM, AFM) revealed extensive layer separation with preserved lateral dimensions. This synergistic approach overcomes the limitations of conventional exfoliation techniques, providing a generalizable and mild route for large-scale production of high-quality, solution-processable h-BN nanosheets for applications in thermal management, dielectric insulation, and advanced nanocomposites.

Supplementary Materials: The following supporting information can be downloaded at: https://www.mdpi.com/article/10.3390/inorganics13100314/s1.

Author Contributions: Methodology, J.H.; Validation, S.-T.L.; Investigation, D.K.; Data curation, S.P. (Seonyou Park); Writing—original draft, S.K.; Writing—review & editing, S.L. and S.P. (Sangyeon Pak). All authors have read and agreed to the published version of the manuscript.

Funding: This work was supported by the National Research Foundation of Korea (NRF) grant funded by the Korea government (Ministry of Science and ICT) (No. RS-2024-00431359 and RS-2024-00411577). This work was also supported by 2025 Hongik University Innovation Support Program Fund.

Institutional Review Board Statement: Not applicable.

Informed Consent Statement: Not applicable.

Data Availability Statement: The original contributions presented in this study are included in the article/Supplementary Material. Further inquiries can be directed to the corresponding author.

Conflicts of Interest: The authors declare no conflict of interest.

References

1. Lim, Y.; Kim, T.; Eom, J.; Harm, O.; Byeon, J.; Lim, J.; Lee, J.; Pak, S.; Cha, S. Two-Terminal MoS2-Based Retinomorphic Devices with Enhanced Synaptic Plasticity. *Adv. Electron. Mater.* **2025**, *11*, 2400878. [CrossRef]
2. Shin, W.; Byeon, J.; Koo, R.H.; Lim, J.; Kang, J.H.; Jang, A.R.; Lee, J.H.; Kim, J.J.; Cha, S.; Pak, S.; et al. Toward Ideal Low-Frequency Noise in Monolayer CVD MoS2 FETs: Influence of van der Waals Junctions and Sulfur Vacancy Management. *Adv. Sci.* **2024**, *11*, 2307196. [CrossRef]
3. Lim, J.; Kim, T.; Park, H.; Eom, J.; Jung, M.; Byeon, J.; Lim, Y.; Pak, S.; Cha, S. Surface Wettability-Mediated Enhancement of Hydrogen Evolution Reaction Performance in Electron-Doped MoS2 Monolayers. *ACS Appl. Energy Mater.* **2024**, *7*, 2938–2945. [CrossRef]
4. Byeon, J.; Eom, J.; Kim, T.; Lim, J.; Jung, M.; Lim, Y.; Park, H.; Hong, J.; Pak, S.; Cha, S. Achieving Adsorbate-Free Monolayered MoS2 Field Effect Transistors by Controlled Surface Gas Treatment. *ACS Appl. Electron. Mater.* **2024**, *6*, 1763–1769. [CrossRef]
5. Pak, S. Controlled p-Type Doping of MoS2 Monolayer by Copper Chloride. *Nanomaterials* **2022**, *12*, 2893. [CrossRef] [PubMed]
6. Wang, J.; Xu, T.; Wang, W.; Zhang, Z. Miracle in "white": Hexagonal boron nitride. *Small* **2024**, *21*, 2400489. [CrossRef]
7. Jiang, P.; Qian, X.; Yang, R.; Lindsay, L. Anisotropic thermal transport in bulk hexagonal boron nitride. *Phys. Rev. Mater.* **2018**, *2*, 064005. [CrossRef]
8. Lu, S.; Shen, P.; Zhang, H.; Liu, G.; Guo, B.; Cai, Y.; Chen, H.; Xu, F.; Zheng, T.; Xu, F. Towards n-type conductivity in hexagonal boron nitride. *Nat. Commun.* **2022**, *13*, 3109. [CrossRef]
9. Wang, J.; Ma, F.; Liang, W.; Sun, M. Electrical properties and applications of graphene, hexagonal boron nitride (h-BN), and graphene/h-BN heterostructures. *Mater. Today Phys.* **2017**, *2*, 6–34. [CrossRef]
10. Cho, J.; Su, P.-C.; Kim, J. Highly thermally conductive and insulating composites fabricated through the hot-pressing of hollow structured h-BN/rGO hybrid filler. *Appl. Mater. Today* **2024**, *37*, 102149. [CrossRef]
11. Liang, L.; Feng, Y.; Yang, K.; Wang, Z.; Zhang, Z.; Chen, X.; Chen, Q. High thermal conductivity electrical insulation composite EP/h-BN obtained by DC electric field induction. *Polym. Compos.* **2024**, *45*, 181–192. [CrossRef]
12. Saji, V.S. 2D hexagonal boron nitride (h-BN) nanosheets in protective coatings: A literature review. *Heliyon* **2023**, *9*, e19362. [CrossRef]
13. Kim, D.I.; Jeong, H.B.; Lim, J.; Jeong, H.S.; Kim, M.K.; Pak, S.; Lee, S.; An, G.H.; Chee, S.S.; Hong, J.P. A Practical Zinc Metal Anode Coating Strategy Utilizing Bulk h-BN and Improved Hydrogen Redox Kinetics. *Energy Environ. Mater.* **2025**, *8*, e12826. [CrossRef]
14. Lim, J.; Heo, S.J.; Jung, M.; Kim, T.; Byeon, J.; Park, H.; Jang, J.E.; Hong, J.; Moon, J.; Pak, S. Highly Sustainable h-BN Encapsulated MoS2 Hydrogen Evolution Catalysts. *Small* **2024**, *20*, 2402272. [CrossRef] [PubMed]
15. Li, J.; Leng, J.; Jiang, Y.; Zhang, J. Experimental characterization of 3D printed PP/h-BN thermally conductive composites with highly oriented h-BN and the effects of filler size. *Compos. Part A Appl. Sci. Manuf.* **2021**, *150*, 106586. [CrossRef]
16. Geim, A.K.; Grigorieva, I.V. Van der Waals heterostructures. *Nature* **2013**, *499*, 419–425. [CrossRef]
17. Pyo, J.; Lim, J.; Byeon, J.; Park, S.; Kang, S.; Park, S.; Lee, S.-T.; Kim, E.; Kim, M.K.; Sohn, J.I. Etchant-Free Wafer-Scale 2D Transfer and van der Waals 3D Integration via Peel-Off Force Engineering. *ACS Nano* **2025**, *19*, 25860–25869. [CrossRef] [PubMed]
18. Deepika; Li, L.H.; Glushenkov, A.M.; Hait, S.K.; Hodgson, P.; Chen, Y. High-efficient production of boron nitride nanosheets via an optimized ball milling process for lubrication in oil. *Sci. Rep.* **2014**, *4*, 7288. [CrossRef] [PubMed]
19. Mittal, N.; Kedawat, G.; Kanika; Gupta, S.; Kumar Gupta, B. An Innovative Method for Large-Scale Synthesis of Hexagonal Boron Nitride Nanosheets by Liquid Phase Exfoliation. *ChemistrySelect* **2020**, *5*, 12564–12569. [CrossRef]
20. Zhao, G.; Zhang, F.; Wu, Y.; Hao, X.; Wang, Z.; Xu, X. One-step exfoliation and hydroxylation of boron nitride nanosheets with enhanced optical limiting performance. *Adv. Opt. Mater.* **2016**, *4*, 141–146. [CrossRef]

21. Yuan, F.; Guan, Q.; Dou, X.; Yang, H.; Hong, Y.; Xue, Y.; Cao, Z.; Li, H.; Xu, Z.; Qin, Y. High-yield synthesis of hydroxylated boron nitride nanosheets and their utilization in thermally conductive polymeric nanocomposites. *RSC Adv.* **2024**, *14*, 21230–21240. [CrossRef] [PubMed]
22. Ren, J.; Stagi, L.; Innocenzi, P. Hydroxylated boron nitride materials: From structures to functional applications. *J. Mater. Sci.* **2021**, *56*, 4053–4079. [CrossRef]
23. Li, G.; Ma, Y.; Xu, H.; Chen, L.; An, Y.; Gao, M.; Zhou, H.; Chen, J. Hydroxylated hexagonal boron nitride nanoplatelets enhance the mechanical and tribological properties of epoxy-based composite coatings. *Prog. Org. Coat.* **2022**, *165*, 106731. [CrossRef]
24. Li, Z.; Li, K.; Li, Y.; Yu, Y.; Lv, J.; Liu, X.; Guan, K.; Lei, W.; Zhang, S.; Zhang, H. Modified molten salt assisted exfoliation of large-size 2D materials. *Adv. Funct. Mater.* **2024**, *34*, 2310371. [CrossRef]
25. Chen, Y.; Kang, Q.; Jiang, P.; Huang, X. Rapid, high-efficient and scalable exfoliation of high-quality boron nitride nanosheets and their application in lithium-sulfur batteries. *Nano Res.* **2021**, *14*, 2424–2431. [CrossRef]
26. Zuo, K.; Zhang, X.; Huang, X.; Oliveira, E.F.; Guo, H.; Zhai, T.; Wang, W.; Alvarez, P.J.; Elimelech, M.; Ajayan, P.M. Ultrahigh resistance of hexagonal boron nitride to mineral scale formation. *Nat. Commun.* **2022**, *13*, 4523. [CrossRef]
27. Coleman, J.N.; Lotya, M.; O'Neill, A.; Bergin, S.D.; King, P.J.; Khan, U.; Young, K.; Gaucher, A.; De, S.; Smith, R.J. Two-dimensional nanosheets produced by liquid exfoliation of layered materials. *Science* **2011**, *331*, 568–571. [CrossRef]
28. Smith, L.; Wei, Z.; Williams, C.D.; Chiricotto, M.; Pereira da Fonte, C.; Carbone, P. Relationship between Capillary Wettability, Mass, and Momentum Transfer in Nanoconfined Water: The Case of Water in Nanoslits of Graphite and Hexagonal Boron Nitride. *ACS Appl. Mater. Interfaces* **2024**, *16*, 56316–56324. [CrossRef] [PubMed]
29. Feng, Z.; Lei, Z.; Yao, Y.; Liu, J.; Wu, B.; Ouyang, W. Anisotropic interfacial force field for interfaces of water with hexagonal boron nitride. *Langmuir* **2023**, *39*, 18198–18207. [CrossRef]
30. Kim, J.; Kwon, S.; Cho, D.-H.; Kang, B.; Kwon, H.; Kim, Y.; Park, S.O.; Jung, G.Y.; Shin, E.; Kim, W.-G. Direct exfoliation and dispersion of two-dimensional materials in pure water via temperature control. *Nat. Commun.* **2015**, *6*, 8294. [CrossRef]
31. Gao, S.; Wang, X.; Song, C.; Zhou, S.; Yang, F.; Kong, Y. Engineering carbon-defects on ultrathin g-C3N4 allows one-pot output and dramatically boosts photoredox catalytic activity. *Appl. Catal. B Environ.* **2021**, *295*, 120272. [CrossRef]
32. Yang, F.; Tang, J.; Ou, R.; Guo, Z.; Gao, S.; Wang, Y.; Wang, X.; Chen, L.; Yuan, A. Fully catalytic upgrading synthesis of 5-Ethoxymethylfurfural from biomass-derived 5-Hydroxymethylfurfural over recyclable layered-niobium-molybdate solid acid. *Appl. Catal. B Environ.* **2019**, *256*, 117786. [CrossRef]
33. Yang, F.; Shao, B.; Liu, X.; Gao, S.; Hu, X.; Xu, M.; Wang, Y.; Zhou, S.; Kong, Y. Nanosheet-like Ni-based metasilicate towards the regulated catalytic activity in styrene oxidation via introducing heteroatom metal. *Appl. Surf. Sci.* **2019**, *471*, 822–834. [CrossRef]
34. Dong, X.; Yang, Y.; Shen, Y.; Yuan, A.; Guo, Z.; Song, H.; Yang, F. Enabling room-temperature reductive C–N coupling of nitroarenes: Combining homogeneous and heterogeneous synergetic catalyses mediated by light. *Green. Chem.* **2022**, *24*, 4012–4025. [CrossRef]
35. Bai, Y.; Xu, Y.; Sun, L.; Ward, Z.; Wang, H.; Ratnayake, G.; Wang, C.; Zhao, M.; He, H.; Gao, J. Two-dimensional Nanosheets by Liquid Metal Exfoliation. *Adv. Mater.* **2025**, *37*, 2416375. [CrossRef]
36. Wang, S.; Li, W.; Xue, J.; Ge, J.; He, J.; Hou, J.; Xie, Y.; Li, Y.; Zhang, H.; Sofer, Z. A library of 2D electronic material inks synthesized by liquid-metal-assisted intercalation of crystal powders. *Nat. Commun.* **2024**, *15*, 6388. [CrossRef]
37. Nayak, A.P.; Dolocan, A.; Lee, J.; Chang, H.-Y.; Pandhi, T.; Holt, M.; Tao, L.; Akinwande, D. Inversion of the electrical and optical properties of partially oxidized hexagonal boron nitride. *Nano* **2014**, *9*, 1450002. [CrossRef]
38. Zhou, L.; Zhang, B.; Li, F.; Yan, Y.; Wang, Y.; Li, R. Preparation of boron nitride nanosheets by glucose-assisted ultrasonic cavitation exfoliation. *Nanoscale Adv.* **2023**, *5*, 6582–6593. [CrossRef] [PubMed]
39. Kong, D.; Zhang, D.; Guo, H.; Zhao, J.; Wang, Z.; Hu, H.; Xu, J.; Fu, C. Functionalized boron nitride nanosheets/poly (L-lactide) nanocomposites and their crystallization behavior. *Polymers* **2019**, *11*, 440. [CrossRef]
40. Zhu, S.; Li, W.; Yuan, W.; Meng, Y.; Chu, Z.; Gan, W. A facile fabrication of nanocomposites with dual conductive networks based on 3D nickel foam, 1D silver nanowires and 2D boron nitride nanosheets. *J. Mater. Sci. Mater. Electron.* **2023**, *34*, 239. [CrossRef]
41. Vorobyeva, N.; Rumyantseva, M.; Platonov, V.; Filatova, D.; Chizhov, A.; Marikutsa, A.; Bozhev, I.; Gaskov, A. Ga2O3 (Sn) oxides for high-temperature gas sensors. *Nanomaterials* **2021**, *11*, 2938. [CrossRef]
42. Matsumae, T.; Kurashima, Y.; Umezawa, H.; Tanaka, K.; Ito, T.; Watanabe, H.; Takagi, H. Low-temperature direct bonding of β-Ga2O3 and diamond substrates under atmospheric conditions. *Appl. Phys. Lett.* **2020**, *116*, 141602. [CrossRef]
43. Zhang, B.; Wu, Q.; Yu, H.; Bulin, C.; Sun, H.; Li, R.; Ge, X.; Xing, R. High-efficient liquid exfoliation of boron nitride nanosheets using aqueous solution of alkanolamine. *Nanoscale Res. Lett.* **2017**, *12*, 596. [CrossRef] [PubMed]
44. Garro Mena, L.; Hohn, K.L. Modification of hexagonal boron nitride by thermal treatment. *J. Mater. Sci.* **2021**, *56*, 7298–7307. [CrossRef]
45. Abdullah, Y.; Husain, H.; Hak, C.R.C.; Alias, N.H.; Yusof, M.R.; Kasim, N.A.; Zali, N.M.; Mohamed, A.A. A short note on physical properties to irradiated nuclear fuel by means of X-ray diffraction and neutron scattering techniques. In *AIP Conference Proceedings*; AIP Publishing LLC: Melville, NY, USA, 2015; p. 040010.

46. Cudziło, S.; Szermer-Olearnik, B.; Dyjak, S.; Gratzke, M.; Sobczak, K.; Wróblewska, A.; Szczygieł, A.; Mierzejewska, J.; Węgierek-Ciura, K.; Rapak, A. Combustion Synthesis of Functionalized Carbonated Boron Nitride Nanoparticles and Their Potential Application in Boron Neutron Capture Therapy. *Materials* **2024**, *17*, 2438. [CrossRef]
47. Li, D.; Sun, H.; Liu, T.; Jin, H.; Li, Z.; Liu, Y.; Liu, D.; Wang, D. Influence of O2 flow rate on the properties of Ga2O3 growth by RF magnetron sputtering. *Micromachines* **2023**, *14*, 260. [CrossRef]
48. Gonzalez Ortiz, D.; Pochat-Bohatier, C.; Cambedouzou, J.; Bechelany, M.; Miele, P. Exfoliation of hexagonal boron nitride (h-BN) in liquide phase by ion intercalation. *Nanomaterials* **2018**, *8*, 716. [CrossRef] [PubMed]
49. Zhang, C.; Tan, J.; Pan, Y.; Cai, X.; Zou, X.; Cheng, H.-M.; Liu, B. Mass production of 2D materials by intermediate-assisted grinding exfoliation. *Natl. Sci. Rev.* **2020**, *7*, 324–332. [CrossRef]

Disclaimer/Publisher's Note: The statements, opinions and data contained in all publications are solely those of the individual author(s) and contributor(s) and not of MDPI and/or the editor(s). MDPI and/or the editor(s) disclaim responsibility for any injury to people or property resulting from any ideas, methods, instructions or products referred to in the content.